

The underestimation of high pressure in DFT+ U simulation for the wide range cold-pressure of lanthanide metals

Yue-Chao Wang,¹ Bei-Lei Liu,^{1,2} Yu Liu,^{1,*} Hai-Feng Liu,¹ Yan Bi,^{3,4} Xing-Yu Gao,¹ Jie Sheng,^{1,5} Hong-Zhou Song,¹ Ming-Feng Tian,¹ and Hai-Feng Song^{1,†}

¹Laboratory of Computational Physics, Institute of Applied Physics and Computational Mathematics, Beijing 100088, China

²School of Mathematical Sciences, Beijing Normal University, Beijing 100875, China

³Center for High Pressure Science and Technology Advanced Research, Beijing 100094, China

⁴National Key Laboratory for Shock Wave and Detonation Physics,

Institute of Fluid Physics, CAEP, Mianyang 621900, China

⁵Graduate School of China Academy of Engineering Physics, Beijing 100088, China

(Dated: May 2, 2022)

Density functional theory plus U (DFT+ U) is one of the most efficient first-principles methods to simulate the cold pressure properties of strongly-correlated materials. However, the applicability of DFT+ U at ultra-high pressure is not sufficiently studied, especially in the widely-used augmented schemes [such as projector augmented wave (PAW) and linearized augmented plane wave (LAPW)]. This work has systematically investigated the performance of DFT+ U in PAW and LAPW at the pressure up to several hundred GPa for the lanthanide metals, which is a typical strongly-correlated series. We found DFT+ U simulation in PAW exhibits an unphysical underestimation of pressure in high-pressure region, which was not observed in conventional DFT simulation. By delicate analysis and comparison with local-orbital-independent hybrid functional results, we have demonstrated that this unphysical behavior is related to a normalization problem on the local density matrix caused by the overlap of local orbitals in PAW under high pressure. Additionally, we observed a slight underestimating of pressure in correlation correction methods in heavy lanthanides (Tm, Yb and Lu) in high-pressure region comparing with the DFT results without the influence of local orbital overlap, and it might be related to the enhancement of binding between atoms in correlation correction methods at high pressure. Our work reveals the underestimation of high pressure in DFT+ U simulation, analyses two sources of this unusual behavior and proposes their mechanism. Most importantly, our investigation highlights the breakdown of DFT+ U for high pressure simulation in VASP package based on PAW framework.

PACS numbers: 71.15.Ap, 71.27.+a, 91.60.Gf

I. INTRODUCTION

Equation of state (EOS) which describes the states and thermodynamic properties of matter is of great interest in astrophysics, planetary physics, power engineering, controlled thermonuclear fusion, impulse technologies, engineering, and several special applications¹. The cold pressure of EOS is usually reduced from shock wave experiment and calculated from Thomas-Fermi model² with various corrections^{3,4}. It is very necessary to validate the cold pressure by rigorous theoretical models and precision experimental data⁵⁻⁸. Lanthanide materials as typical research objects for high-pressure physics and national defense, its wide-range cold pressure is of especial importance^{9,10}. However, it is still difficult to obtain the high-quality experimental results under extreme cold-pressure conditions. As far as we know, the highest static pressure achieved in lanthanide materials is the recent works on Ho (282 GPa) and Nd (302 GPa), and experimental works with static pressure over 250 GPa are rare^{11,12}. Thus, the simulation becomes further more important to obtain high-pressure data, especially the high precision first-principles methods¹³⁻¹⁵. However, the systematic research on the applicability of these conventional methods is still lack of simulating the

strong-correlated electronic materials, such as lanthanide metals.

Until now, the most successful and widely used first-principles methods are often referred to the Kohn-Sham density functional theory (KS-DFT), and the correction methods based on it^{16,17}. For the simulation of EOS at conventional conditions, many works have proven the capability of KS-DFT on weakly correlated material^{18,19}. Among the implementation techniques of DFT, the augmented methods, such as linearized augmented plane wave (LAPW) and projector augmented wave (PAW) are of most widely usage²⁰⁻²³. LAPW and PAW are now implemented in many famous software packages, e.g. WIEN2k²⁴, Elk²⁵, VASP²⁶, Quantum-Espresso²⁷, GPAW²⁸ and ABINIT²⁹. LAPW and PAW methods are the representatives of high accuracy and high effectiveness in the conventional implementation of KS-DFT respectively³⁰. Another advantage of the augmented methods is that the definition of atomic orbitals is straightforward in these methods. It makes the implementation of correction methods based on local orbitals much easier in the scheme of LAPW and PAW^{26,31}.

For strongly correlated materials, such as lanthanides, the KS-DFT often fails, and correction methods are needed. DFT+ U is one of the most effective correction methods, which is based on local orbitals^{32,33}. DFT+ U

has been successfully used in the simulation of crystal structures, magnetic order, charge order and many other properties related to the total energy^{34,35}. There are other correction methods based on local orbitals, such as DFT plus dynamic mean-field theory (DMFT) and Gutzwiller projected variational wave function^{32,36}. These local-orbital-based corrections can make delicate or effective corrections for the strongly-correlated part (like $4f$ -electron in lanthanides)^{37,38}. Another class of correction methods is non-local-orbital based, such as hybrid functionals. This class of methods makes no bias on the electrons and often with less artificial factor (like the definition of local orbitals)^{39,40}. However, the computational cost of hybrid functional is at least one order larger than DFT and DFT+ U ⁴¹. The simulation of the wide range EOS of the complex materials usually requires tens or hundreds of total energy data points, which is beyond the capability of many sophisticated correction methods. For the calculation of wide range EOS, the most attractive candidate (if not only) is the DFT+ U method, which applies a correction based on static mean-field approximation of the onsite Hubbard model and has a similar computational cost as KS-DFT^{42–45}.

The effectiveness of DFT+ U with PAW and LAPW methods has been just proved in conventional conditions. But there have already been many works considering the strongly correlated effect with DFT+ U performed for high-pressure condition, especially in PAW^{34,46–51}. Many analyses and conclusions are based on these simulations, however, the applicability of DFT+ U for high pressure is still not clear. In DFT+ U methods, many factors can affect its performance, like the double-counting term, interaction strength U and J , and the local orbitals constructed from DFT calculation. Especially for the local orbitals defined in low pressure conditions, the overlap problem at high pressure makes the reliability of local orbitals more suspicious than other factors. In an earlier work, the definition and overlap of the local orbital in VASP has shown a different performance in the Mn dioxides comparing with WIEN2k⁵². This problem may become serious when the distance between atoms is shortened to 80% at pressure over 100 GPa. Although software such as VASP has already warned users about the risk of the overlap, the requirement of the high-pressure simulation still makes researchers to take the risk. Thus, systematic research of the reliability of DFT+ U in high pressure is necessary.

In this work, we investigate the performance of DFT+ U in lanthanide metals at high pressure from two aspects. Firstly, we compare the DFT+ U results from VASP and WIEN2k at the same U and J values at normal pressure and high pressure over 300 GPa, together with a set of results of hybrid functional (HSE06) as a benchmark. From our systematic investigation of the total energy, pressure and electronic structures of lanthanide metals, we find over unphysical softening results given by the DFT+ U with PAW methods. Through our analysis, this over softening connects with the normal-

ization error of local orbitals led by the overlap. We also find the results from higher reliable correction methods like hybrid functional and DFT+ U based on LAPW show a trend of underestimating the pressure in high-pressure region comparing with the DFT. This phenomenon implies besides the technique problem, there may be some physical mechanism.

The paper is organized as follows. In Sec. II we introduce the methods and parameters used in this paper. In Sec. III, the total energy, pressure and electronic structure results of lanthanide metals at different simulation conditions are exhibited. In Sec. IV we analyze the abnormal underestimation of pressure in DFT+ U from the overlap of local orbitals view, and discuss the results in Sec. III from the normalization error led by the overlap and an underestimating of pressure caused by the mechanism of correction methods. In Sec. V we close the paper with a summary of the main finds of this work and some general remarks. In the Appendix, the detailed procedure of definition of local orbitals in LAPW and PAW are shown.

II. METHOD

A. Simulation methods

All 15 kinds of lanthanide metals investigated in this work are the face centered cubic (FCC) structure, which is a conventional close-packed structure for lanthanide metals. Since the main purpose of this work is to reveal the capability of DFT+ U method to simulate metals with $4f$ electrons under high-pressure, the other probable structures are not considered in this work. To include both low and ultra-high pressure, the volumes we considered are from 9 \AA^3 to 28 \AA^3 . PAW and LAPW simulations are performed in VASP²⁶ and WIEN2k²⁴ packages respectively, and we specially refer PAW (LAPW) results to VASP (WIEN2k) simulations in this work. The exchange-correlation functional used for all calculations is generalized gradient approximation (GGA) of Perdew-Burke-Ernzerhof formation (PBE)⁵³. A grid of $17 \times 17 \times 17$ is used for the k-spacing sampling. The pseudo-potentials used for PAW simulation are recommended by VASP, which means the $5s$, $5p$, $5d$, $4f$ and $6s$ are treated as valence for all lanthanides. And the cutoff energy of plane wave is 600 eV, which is large enough for calculation of energy and force for all conditions in this work. The augmentation radius of all $4f$ elements in LAPW calculation is 1.11 Å (2.1 bohr.), and the $R_{k\text{max}}$. The “+ U ” correction takes the isotropic form to reduce the number of parameters. The U_{eff} (or the $U - J$ in some context) is 5.0 eV for all lanthanide elements, and the double-counting term is “fully localized limit” (FLL), which is the rational option for many DFT+ U works^{54,55}. For comparison, hybrid functional calculations using HSE (Heyd-Scuseria-Ernzerhof) formation are performed in VASP⁵⁶. Since spin-polarization

can drastically change the electronic states between different methods and makes the comparison much complicated, no spin-polarization is considered in this work. For the calculation of pressure, each energy-volume curve is fitted by Birch-Murnaghan equation with 50 sampling points in the range from 9 \AA^3 to 28 \AA^3 .

B. Projection of local orbits

In the “+ U ” correction, besides the correlation strength U_{eff} and double-counting term, one of the most important factors is the definition of local Hilbert space which the model Hamiltonian is worked on⁵⁷. From the technical point of view, a set of local orbitals is often used to define this local subspace. By acting the projection operator $\hat{P}(\mathbf{r}, \mathbf{r}')$ composed by the local orbitals on the whole Hilbert space, the local density matrix can be obtained⁵². There are three kinds of most common formations of the projection operator: spherical augmented schemes, atomic orbitals and special functions (e.g. Wannier function)^{31,58-60}. As the simulation tools of materials based on augmented basis sets (e.g. VASP and WIEN2k) are widely used, many works of “+ U ” correction are carried out with spherical augmented projection operator. The details of projection operators in PAW and LAPW and how they act on the single electron orbitals to obtain local density matrix are described in the appendix part.

III. RESULTS

A. Pressure in different methods

The results of lanthanide metals’ pressure at large (upper panel, 28 \AA^3) and small (lower panel, 9 \AA^3) volume in different simulation conditions are shown in Fig.1. The simulation condition we considered includes DFT (PBE, green bar) and “+ U ” correction (red bar) in PAW and LAPW methods, and the HSE06 hybrid functional (blue bar) based on PAW. HSE06 is used as a benchmark, considering hybrid functional is not directly dependent on the local orbitals as “+ U ” correction, and the level of correction of correlation effect is not lower than the “+ U ” correction. Two important features are exhibited in Fig.1. Firstly, an abnormal high-pressure softening of the results from DFT+ U in PAW can be observed. In high pressure conditions, the pressure of some heavy lanthanide metals is underestimated by 50% to 80% in DFT+ U simulation from PAW comparing with that from LAPW. Meanwhile, in low pressure conditions, the DFT+ U results between PAW and LAPW are similar. Secondly, the pressure calculated by DFT is higher than the correlation correction methods (both “+ U ” and HSE06) in some heavy lanthanide metals (Tm, Yb and Lu). It is contrary to the general experience of

these correction methods that “+ U ” and hybrid functional often give a higher pressure comparing to DFT at the same volume, as can be observed in our results of low-pressure condition^{40,52,54,55}. For the first feature mentioned above, it can be found that the PAW pseudo-potential is not the reason of the abnormal softening of pressure from DFT+ U in PAW, since both in high and low pressure the DFT results from LAPW and PAW are similar. The “+ U ” correction also should not be accused for these abnormal results, since HSE06 and “+ U ” correction in LAPW give similar results in both low and high pressure. The answer to the unreasonable results of “+ U ” correction in PAW under high pressure seems only related to the implementation of “+ U ” correction in PAW. The main difference of implementation “+ U ” in PAW and LAPW is that the overlap between augmented sphere in PAW cannot be avoided, since the radius of the sphere is fixed when the pseudo-potential is created in PAW. Other results connecting with the abnormal behavior of PAW in high-pressure condition is shown in the following, and a detailed analysis is also presented. For second feature that the pressure described by DFT is higher than that of correlation correction in high-pressure conditions, it may relate to the theoretical mechanism behind correlation correction methods other than the implementation problem, since the phenomenon exhibits in both HSE06 and “+ U ” simulation. We give our interpretation of the phenomenon in the discussion.

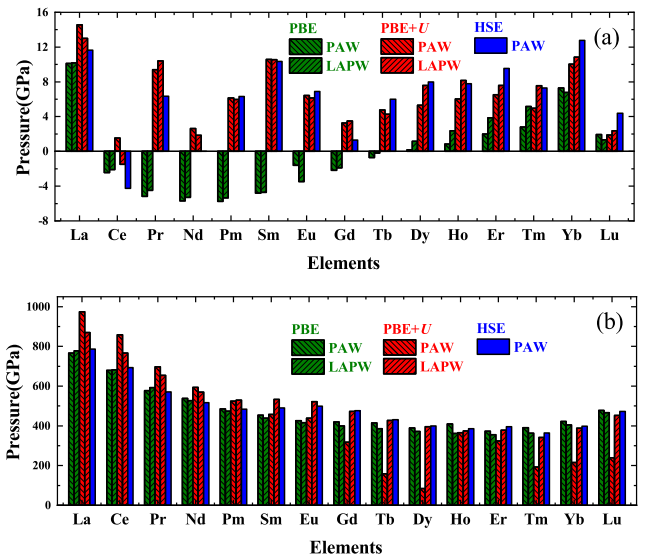


FIG. 1: The pressure calculated with different methods at large volume (28 \AA^3 , panel a) and small volume (9 \AA^3 , panel b) of lanthanide metals with FCC structure. The green bars stand for the results from DFT (PBE functional), the red bars stand for the results from DFT+ U ($U_{\text{eff}} = 5.0 \text{ eV}$), and the blue bars stand for the results from HSE06. The VASP and Wien2k results are mark by shadow with backslash and slash respectively.

B. Energy, Pressure and Modulus versus volume

In this subsection, the “+ U ” results of total energy, pressure and modulus changing versus volume (simplified to E-V, P-V and B-V in the work respectively) are displayed in PAW and LAPW. The E-V, P-V and B-V results are calculated in the range from 9 \AA^3 to 26 \AA^3 . We have checked the pressure from the Hellmann-Feynman (reading from the software report) and from energy difference, and the results are the same. It should be mentioned here, the zero point of the total energy of each system is set as the energy of 9 \AA^3 . For the simulation in this subsection, we display the results of La, Gd and Yb, since these three lanthanide metals represent three kinds of $4f$ -occupation conditions, the empty occupation La, half occupation Gd and full occupation Yb. The Fig.2 shows the E-V, P-V and B-V results of La, Gd, and Yb. For La, the E-V results from PAW always change fast comparing to LAPW with volume decreasing. This is obvious in the P-V results, for pressure can be seen as the first derivative of energy with respect to volume. In the P-V results of La, the pressure of PAW is always large than that of LAPW at every volume point. However, it can be observed that the difference of pressure between PAW and LAPW is decreasing with the decreasing of volume. In the B-V results (the second derivative of energy with respect to volume), the difference between PAW and LAPW is almost vanishing at the small volume. For half occupation system Gd, with the decrease of volume, the total energy of PAW increases faster than LAPW below 100 GPa. At higher pressure, results of LAPW increase faster. In the P-V results, curves of PAW and LAPW cross at about 100 GPa in Gd. These crossings happen at a much larger volume in the B-V results of Gd. For the nearly fully occupied Yb, the variation of energy versus volume in PAW and LAPW is similar in low pressure. In P-V results, the pressure of LAPW is larger than PAW results at every volume point, and at the volume of 9 \AA^3 , the difference can be as large as 150 to 200 GPa, which has a relative difference larger than 50%. For the B-V results, PAW gives smaller values comparing with LAPW, and an abnormal phenomenon is observed that modulus from PAW starts to decrease with the decreasing of volume at high pressure.

C. Electronic structures

The “+ U ” correction of electronic structures at low and high pressure is investigated in this subsection. We also choose La, Gd and Yb as representatives for empty, half-filling and full occupied f -shell. The band structures calculated by the “+ U ” correction in PAW and LAPW are shown in Fig.3. At low pressure, it can be observed that the electronic structures from PAW and LAPW are similar, especially the itinerant bands below the Fermi level. For the local f -bands, the results of PAW and LAPW show the difference about 0.1 eV. The

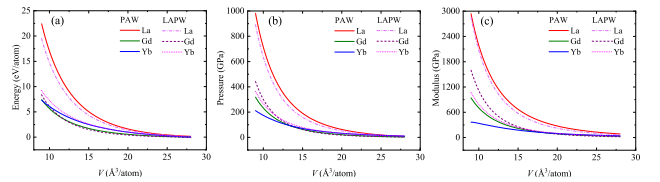


FIG. 2: The results of total energy (a), pressure (b) and modulus (c) versus volume from DFT+ U in 6 typical lanthanide metals. Lower occupied systems (La) are red solid line (PAW) and violet dot-dashed line (LAPW). Half occupied systems (Gd) are green solid line (PAW) and purple dashed line (LAPW). Full occupied systems (Yb) are blue solid line (PAW) and pink dotted line (LAPW). The zero point of total energy is set as the energy of the smallest volume (9 \AA^3).

PAW results give lower f -bands below the Fermi level than LAPW results. At high pressure, the difference of electronic structures calculated from PAW and LAPW becomes larger. Besides all bands becoming more dispersed, PAW still makes the f -bands far away from the Fermi level comparing to LAPW, but the detailed features become much more complicated. However, it seems no qualitative difference between PAW and LAPW electronic structures at high pressure.

IV. DISCUSSION

A. Total Energy and Occupation

To understand the abnormal pressure feature shown in the results of “+ U ” in the PAW method, we should analyze how “+ U ” correction makes an influence on the total energy. It is because the pressure reflects the changing of total energy versus volume. The total energy of DFT+ U is

$$E_{\text{DFT}+U}[\rho(\mathbf{r}), \{n\}] = E_{\text{DFT}}[\rho(\mathbf{r})] + E_U[n] - E_{\text{dc}}[n]. \quad (1)$$

In this work, all formations of “+ U ” correction are shown on a diagonalized local density matrix. On one hand, it can make the analysis more clear. On the other hand, for the examples in this work, the diagonal part gives the major contribution to the results. The double counting of FLL form is adopted, which is

$$E_{\text{dc}}^{\text{FLL}} = \frac{U}{2}N(N-1) - \sum_{\sigma} \frac{J}{2}N_{\sigma}(N_{\sigma}-1). \quad (2)$$

Without the anisotropic effect, the total energy correction in “+ U ” is

$$\Delta E_{\text{DFT}+U} = \frac{U_{\text{eff}}}{2} \sum_{m,\sigma} [n_m^{\sigma} - (n_m^{\sigma})^2]. \quad (3)$$

Since in most of the “+ U ” works, the U_{eff} is constant, n_m^{σ} the occupation of local orbitals, becomes the key factor that affects the total energy.

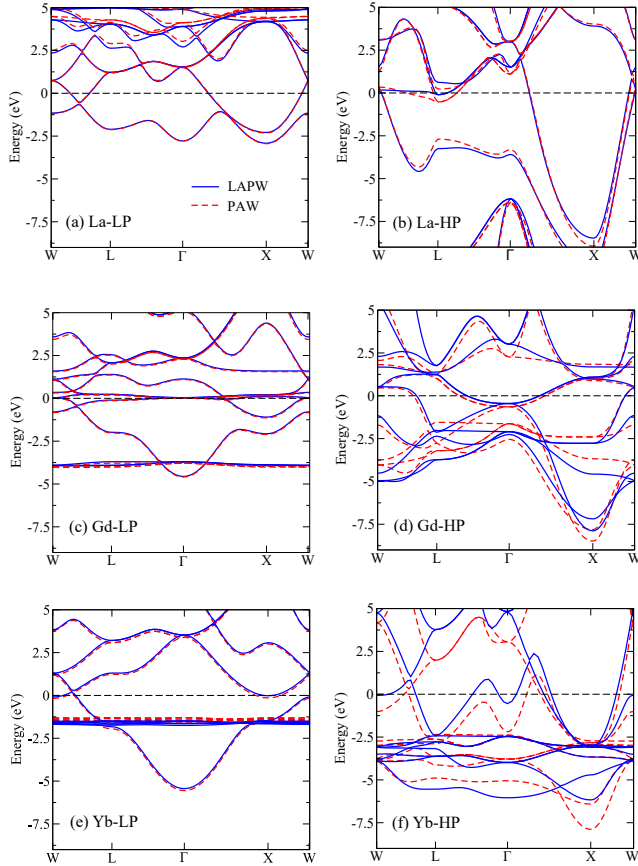


FIG. 3: The electronic band structure calculated by DFT+ U in VASP (red dashed line) and WIEN2k (blue solid line) of La (a,b), Gd (c,d) and Yb (e,f) at low pressure (LP) and high pressure (HP).

The n should have a value between 0 and 1 from the definition of the occupation of local orbitals. It is because n_{mm} is

$$n_{mm} = \sum_{i \in occ} \langle m | \psi_i \rangle \langle \psi_i | m \rangle. \quad (4)$$

ψ_i is KS orbital, and the summation is over all occupied orbitals. For the completeness of the KS orbitals, all the KS orbitals can construct a unit operator

$$\hat{I} = \sum_i |\psi_i\rangle \langle \psi_i|. \quad (5)$$

Thus, it can be written out like

$$\begin{aligned} \langle m | m \rangle &= \sum_i \langle m | \psi_i \rangle \langle \psi_i | m \rangle \\ &= \sum_{i \in occ} \langle m | \psi_i \rangle \langle \psi_i | m \rangle + \sum_{i \notin occ} \langle m | \psi_i \rangle \langle \psi_i | m \rangle. \end{aligned} \quad (6)$$

So,

$$n_{mm} = \langle m | m \rangle - \sum_{i \notin occ} \langle m | \psi_i \rangle \langle \psi_i | m \rangle \quad (7)$$

Because $\sum_{i \notin occ} \langle m | \psi_i \rangle \langle \psi_i | m \rangle \geq 0$, n_{mm} should little than $\langle m | m \rangle$. If $|m\rangle$ is a well-defined atomic orbital, it should satisfy the normalization condition that $\langle m | m \rangle = 1$, and we can make a conclusion that $n_{mm} \leq 1.0$.

For the n with value in range 0 to 1 and $U_{eff} > 0.0$ (electrons repulse with each other), the “+ U ” correction with FLL double counting term gives an energy correction larger than 0.0. This correction becomes 0 only if n equals 1 or 0. This feature of “+ U ” correction has been reported in previous works. Another well-known feature is that lower orbital energy is obtained with occupation larger than 0.5⁶¹.

B. Occupation problem in PAW

In our PAW simulations, the occupation of some local density matrix elements exceeds 1.0, and we investigate the origin and influence of the phenomenon through the variation of local density matrix with the pressure (or volume). $\Delta N_{>1}$ is defined as the summation of all local orbitals which is more than 1.0, and has the form

$$\Delta N_{>1} = \sum_{m=-3}^3 \begin{cases} n_{mm} - 1.0 & n_{mm} > 1 \\ 0.0 & n_{mm} \leq 1. \end{cases} \quad (8)$$

n_{mm} are the diagonal elements of the local density matrix, and the summation of m from -3 to 3 means all 7 orbitals in 4*f* shell (spin polarization is not considered).

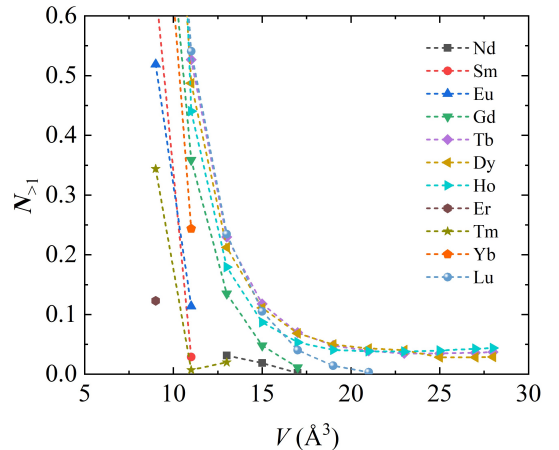


FIG. 4: The over 1.0 part of the local orbital occupation of the lanthanide metals versus volume in the VASP DFT+ U calculation. The systems without any local orbital occupation over 1.0 (La, Ce, Pr) are not shown in the figure.

As shown in Fig.4, except for some elements with lower occupation (like, La, Ce, Pr), the occupation of most

lanthanide metals can show obvious exceeding over 1.0. The systems with occupation over 1.0 can be divided into two kinds. One is that the occupation of some orbitals is over 1.0 even at low pressure (Tb, Dy, Ho). These systems correspond to the first dipping of pressure in serial of lanthanide metals in high pressure results. In the other kind occupation only exceeds 1.0 when the pressure is high enough. No matter which kind of behavior, as we have discussed above, the occupation of local orbital exceeding 1.0 happens only in two conditions: The normalization of KS orbitals is not satisfied, or the modular square of local orbitals has problem. As the DFT results of PAW and LAPW are similar, the KS-orbital should be normalized correctly. We also have tested the modular square of KS-orbitals dominated by f -feature, and the normalization can be achieved at 10^{-8} level. To analyse the local orbitals, we split the modulus square of PAW orbitals into several parts. The modular square of the PAW orbitals writes

$$\begin{aligned} \langle \psi_i | \psi_i \rangle &= \langle \tilde{\psi}_i | \tilde{\psi}_i \rangle \\ &+ \sum_{ss'} \langle \tilde{\psi}_i | \tilde{p}_s \rangle \left(\langle \phi_s | \phi_{s'} \rangle - \langle \tilde{\phi}_s | \tilde{\phi}_{s'} \rangle \right) \langle \tilde{p}_{s'} | \tilde{\psi}_i \rangle. \end{aligned} \quad (9)$$

$|\phi_s\rangle$ and $|\tilde{\phi}_s\rangle$ are the all-electron partial orbital and pseudo partial orbital of the same atom respectively. $|\psi_i\rangle$ and $|\tilde{\psi}_i\rangle$ are all-electron orbital and pseudo-orbital and these two terms are connected by a projector $|\tilde{p}_s\rangle$. In usual case, $|\phi_s\rangle$, $|\tilde{\phi}_s\rangle$ and $|\tilde{p}_s\rangle$ is fixed as a certain pseudo-potential is used, while $|\psi_i\rangle$ and $|\tilde{\psi}_i\rangle$ are renewed at each self-consistent cycle. The subscript s stands for a collection of orbital momentum l and m , and the site of atom. Here we split it into three parts: integral of pseudo-orbital on plane wave

$$\tilde{\mathcal{S}}_{i,pw} = \langle \tilde{\psi}_i | \tilde{\psi}_i \rangle, \quad (10)$$

integral of pseudo atomic orbital

$$\begin{aligned} \tilde{\mathcal{S}}_{i,atom} &= \sum_l \tilde{\mathcal{J}}_{i,atom}^{lm} \\ \tilde{\mathcal{J}}_{i,atom}^{lm} &= \sum_{s \in lm; s' \in lm} \langle \tilde{\psi}_i | \tilde{p}_s \rangle \langle \tilde{\phi}_s | \tilde{\phi}_{s'} \rangle \langle \tilde{p}_{s'} | \tilde{\psi}_i \rangle. \end{aligned} \quad (11)$$

and integral of all-electron atomic orbital

$$\begin{aligned} \mathcal{S}_{i,atom} &= \sum_{lm} \mathcal{J}_{i,atom}^{lm} \\ \mathcal{J}_{i,atom}^{lm} &= \sum_{s \in lm; s' \in lm} \langle \psi_i | \tilde{p}_s \rangle \langle \phi_s | \phi_{s'} \rangle \langle \tilde{p}_{s'} | \psi_i \rangle. \end{aligned} \quad (12)$$

With this splitting, the integral of PAW orbital can be written as

$$\langle \psi_i | \psi_i \rangle = \tilde{\mathcal{S}}_{i,pw} + \mathcal{S}_{i,atom} - \tilde{\mathcal{S}}_{i,atom}. \quad (13)$$

Considering the definition of the diagonal element of local density matrix n_{mm} ,

$$n_{mm} = \sum_{i \in occ} \mathcal{J}_{i,atom}^{lm}. \quad (14)$$

If n_{mm} is fully contributed by one occupied KS-orbital ψ_i , $n_{mm} = \mathcal{J}_{i,atom}^{lm}$. The interval part of the integral is $\tilde{\mathcal{S}}_{i,pw} - \tilde{\mathcal{S}}_{i,atom}$, and the atom part of the integral is $\mathcal{S}_{i,atom}$. The interval and atom part of the integral stand for the probability to find the electron on orbital in the interval and augmented region respectively.

As we have shown, the all-electron atomic orbital has a close relation to the local orbital. And we can investigate the normalization of local orbital by the modular square of all-electron atomic orbital. From the physical meaning of orbital, $\mathcal{S}_{i,atom}$ should be less than 1.0, otherwise there is something abnormal happened to the local orbital. We analyze this problem at high pressure in PAW method in Yb as an example, since the abnormal behavior in high-pressure simulation is obvious in the heavy lanthanides. It should be clarified that the occupation defined in Eq.4 is not the exact case in augmented methods. However, if a case with only one type of radial orbital for each shell is considered, the occupation defined in Eq.4 could be equivalent with the augmented methods.

Here we consider a simplified situation, where only one kind of radial part $|R_l\rangle$ is used for the shell l in each site. In this way, it is easier to compare the difference between occupation matrix elements obtained from augmented methods and the ones from projecting onto a set of local orbital $|m\rangle$, as shown in Eq.4 The occupation matrix elements in augmented methods become,

$$n_{mm'}^{aug} = \sum_{i \in occ.} \langle \tilde{\psi}_i | \tilde{p}_m \rangle \langle \tilde{p}_{m'} | \tilde{\psi}_i \rangle \langle R_l | R_l \rangle. \quad (15)$$

$n_{mm'}^{aug}$ stands for an occupation matrix element in PAW, and a general form of it is provided in appendix. The occupation matrix elements obtained by projecting onto local orbitals are,

$$n_{mm'}^{proj} = \sum_{i \in occ.} \langle \tilde{\psi}_i | \tilde{p}_m \rangle \langle \tilde{p}_{m'} | \tilde{\psi}_i \rangle |\langle R_l | R_l \rangle|^2. \quad (16)$$

$n_{mm'}^{proj}$ is the occupation matrix element from the procedure defined in Eq.4, and the radial part of local orbital $|R_l\rangle$ takes the same function as the all-partial orbital in PAW. It can be clearly observed that if the radial parts of the shell has the same shape, and the local orbital is well normalized, $n_{mm'}^{aug} = n_{mm'}^{proj}$.

In the table I, we show the different parts of orbital integral of Yb at low and high pressure at Γ point of reciprocal space. As in the “+ U ” correction of Yb, almost all f -feature bands are below the Fermi energy, the $\mathcal{S}_{i,atom}$ and $\tilde{\mathcal{S}}_{i,atom}$ are almost contributed by $\mathcal{J}_{i,atom}^{fm}$, and the 7 orbitals listed in the table are the ones with obvious f -feature. At low pressure, the integral results perform normally. A finite positive value shows for every

part, and the summation of all parts equals 1.0. At high pressure, though the summation of all parts is still 1.0, there shows some abnormal features. The part of the augmented region is over 1.0, and the interval region has negative values. These features are consistent with the occupation of local orbitals over 1.0 at high pressure and imply a normalization problem of the local orbital.

The drastic changes of $\mathcal{S}_{i,atom}$ and $\tilde{\mathcal{S}}_{i,atom}$ between low-pressure and high-pressure conditions implies a variation of the wave function radial part with pressure in the augmented region. In VASP, there are two predefined radial functions forming the basis to describe the f-shell. We show these radial functions in Fig.5. The blue solid line represents a radial function with typical 4f-feature (localized around core, one peak and decaying to zero at distance), and we labeled it by F_1 . The red dashed line represents a radial function more divergent, we labeled it by F_2 . The black vertical dashed line labeled by R_c stands for the radius of the augmented region. The sudden drop of F_2 is a truncation, and since it is out of the R_c , we believe it doesn't affect the results directly.

TABLE I: The components of the module square integral of KS orbitals with 4f feature at Gamma point in Yb metal in low pressure (LP) and high pressure (HP) conditions

No.	$\mathcal{S}_{i,atom}$		$\tilde{\mathcal{S}}_{i,atom}$		$\mathcal{S}_{i,pw} - \mathcal{S}_{i,atom}$	
	LP	HP	LP	HP	LP	HP
1	0.9803	1.3998	0.0601	0.6521	0.0197	-0.3998
2	0.9904	1.0474	0.0482	0.1359	0.0096	-0.0508
3	0.9904	1.0474	0.0482	0.1359	0.0096	-0.0508
4	0.9904	1.0474	0.0482	0.1359	0.0096	-0.0508
5	0.9991	1.0114	0.0345	0.0199	0.0009	-0.0114
6	0.9991	1.0114	0.0345	0.0199	0.0009	-0.0114
7	0.9991	1.0114	0.0345	0.0199	0.0009	-0.0114

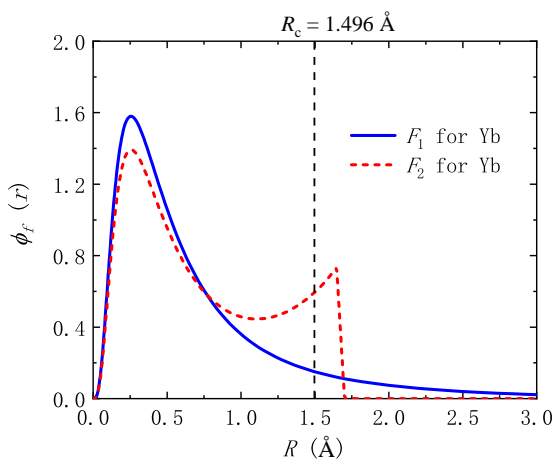


FIG. 5: Two prefixed the radial f orbitals (F_1 and F_2) of all-electron in the Yb PAW pseudo-potential of VASP (blue solid line and red dashed line). R_c stands for the augmented range of PAW, which is a range of projection operator in DFT+U.

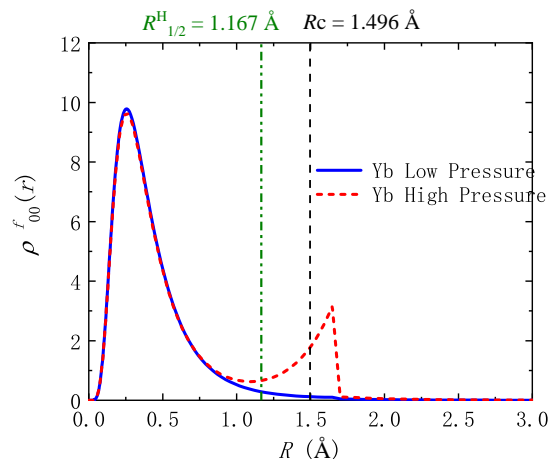


FIG. 6: The spherical averaged radial charge distribution of Yb at low pressure (blue solid line) and high pressure (red dashed line). $R_{1/2}^H$ is half of the distance between the closest atoms in high pressure. R_c stands for the augmented range of PAW.

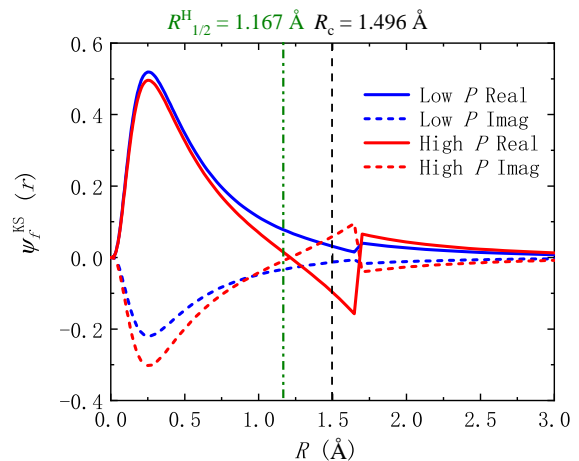


FIG. 7: The radial part of a KS orbital with f feature of Yb at low pressure (blue lines) and high pressure (red lines). The solid line and the dashed line stand for real and imaginary part of the orbital respectively. $R_{1/2}^H$ is half of the distance between the closest atoms in high pressure. R_c stands for the augmented range of PAW.

In Fig.6, the average of radial charge distribution of 4f orbital in Yb over a spherical surface is shown at low (blue solid line) and high pressure (red dashed line). The $R_{1/2}^H$ is the half of the distance between the nearby atoms at high pressure, which stands for the radial not overlap. The radial charge can reflect the shape of the local orbital. It can be observed that when R is smaller than $R_{1/2}^H$, the charge distributions of low and high pressure are both similar to the shape of F_1 . When in the range between $R_{1/2}^H$ and R_c , the high-pressure result shows are

divergent feature like F_2 . The divergent F_2 feature leading to additional electrons in the range between $R_{1/2}^H$ and R_c . The charge distribution in high-pressure with F_2 feature implies the local orbital lost the typical characteristic of $4f$ like F_1 .

The Fig.7 shows two radial parts of local orbital functions of Yb at low and high pressure respectively. These local orbitals are from the occupied KS-orbitals close to the Fermi energy at Gamma point, which are almost f -feature. It can be clearly seen that at low pressure (blue lines), the orbital shows a typical $4f$ -feature as F_1 , and almost no F_2 feature expresses. For the orbital at high pressure, an F_2 feature shows in the range $R_{1/2}^H$ and R_c , which is consistent with the charge distribution results. Another important feature of the high-pressure orbital is that a “node” appears just at the position $R_{1/2}^H$. It reveals a probable explanation for the occupation over 1.0. The overlap of the augmented sphere leads to the invasion of the nearest orbital, and makes the feature far from typical $4f$. Then, the weight of F_2 becomes larger at the projection operator. The feature of $4f$ near the nucleus still needs to be described with F_1 . At last, the excessive F_2 component together with the F_1 leads to an over 1.0 occupation.

C. Abnormal behavior of “+ U ” in PAW

It is demonstrated that the overlap of local orbital in PAW can cause an abnormal local density matrix, and one can explain the abnormal behavior of simulation results by PAW from this point of view. For the E-V, P-V and B-V results, the LAPW results increase faster with the decreasing of the volume than PAW. It is the results of total energy correction with FLL double counting term and local density matrix difference between PAW and LAPW. There are two different conditions. One is the occupation of every local orbital is lower than 0.5 (as in La). In this condition, the total energy grows faster when the occupation of the local density matrix grows faster, and the P-V and B-V become steeper at a small volume. The other condition is that all local orbitals are over 0.5 occupations (as in Yb). At this condition, the total energy grows slower when the occupation of the local density matrix grows faster, and the P-V, B-V becomes less steep at a small volume. The case between these two conditions (as in Gd) leads to the cross of E-V, P-V and B-V curves between PAW and LAPW results. Since the DFT results of PAW and LAPW are similar at both low and high-pressure conditions, the contribution from the DFT part to the total energy in DFT+ U is similar. The main difference between the DFT+ U results of PAW and LAPW comes from the “+ U ” correction. The “+ U ” correction based on PAW in VASP has a larger projection range, thus more electrons are counted in the local density matrix. Together with the overlap of local orbital, the local orbital occupation increases faster in PAW than it in the LAPW with the decreasing of volume. It makes

the “+ U ” correction shows a more obvious effect in PAW results, which may even lead to an unphysical result.

For the abnormal behavior of Yb in PAW results, that the B-V results show a decrease with the volume decreasing, it is caused by a similar mechanism as above. In the high press condition of Yb, the occupation of local orbitals is all over 1.0 in PAW. As having been introduced at the beginning of this part, the contribution of the “+ U ” correction of energy becomes negative when the occupation is over 1.0. With the volume decreasing and the occupation of $4f$ increasing, the negative contribution to the total energy in Yb becomes remarkable. This negative contribution from the “+ U ” correction suppresses a normal trend described by the DFT part. The P-V should also show a similar behavior in the PAW, if the volume is smaller.

The difference of electron structure results between PAW and LAPW can be explained from two aspects. Firstly, the large local orbital range in PAW has more weight in the KS orbital than LAPW dose. And it makes “+ U ” correction in PAW has more influence on the band structure. Secondly, the large projection range in PAW makes more occupation on the local orbitals, and more occupation means lower orbital energy in “+ U ” correction. It leads to a lower band energy in occupied orbitals in PAW. Though the electron structure results of PAW and LAPW show some differences, no obvious qualitative difference as in the E-V, P-V and B-V results has been captured. It may be understood from the fact that the “+ U ” correction of orbital is linear, but the correction of total energy is quadratic.

D. Underestimation of pressure in correction methods

Another phenomenon observed above is that the DFT predicts higher pressure than other correction methods in small volume (high-pressure) range for Tm, Yb and Lu. This underestimating of pressure appears in all correction methods we tested. Similar results are reported in many “+ U ” and hybrid functional works at ambient pressure, where the correction methods give a larger volume and a smaller bulk modulus comparing with the DFT results^{62,63}.

A usual interpretation for this phenomenon is that the correction methods make the correlation electrons more concentrated around the nuclei which leads the atoms behaving like isolated atoms. The isolated behavior causes the binding between the atoms are weakened, and induce a larger volume and a smaller bulk modulus. However, in high-pressure condition with hundreds of gigapascals, the isolated atom interpretation may failed. We propose a qualitative understanding for the phenomenon in high-pressure range from the point that the capability of localizing electrons in HSE06 and “+ U ” may increase the binding between atoms. Different from the condition at ambient pressure, when the volume is small enough,

there is not much space for the f electrons concentrated around the atoms. The electrons may prefer to localize between atoms, and the correction methods still can stabilize these local electrons. The concentration of electrons between atoms can binding the nucleus tight, which seems like some kind of “bonding effect”. This effect makes the correction methods to predict a much smaller volume in high-pressure condition, or smaller pressure with the same volume. An illustration try to explain the picture is shown in Fig.8 schematically. However, it is just a rough interpretation qualitatively, and more detailed investigation is required for clearly understanding the results.

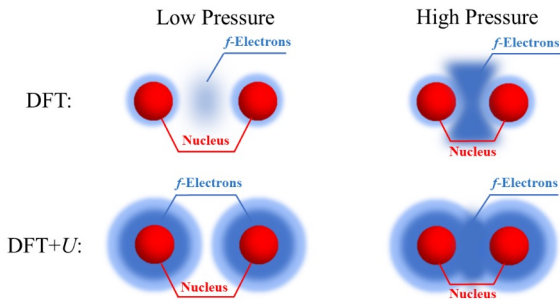


FIG. 8: The diagram about the underestimation of pressure in correlation correction comparing with the common DFT. The upper panel shows that in DFT, the electron density increases uniformly when the pressure becomes higher. The lower panel shows the correction methods (as DFT+ U) stabilize the electron in the interatomic region in the high-pressure condition, which leads to a binding trend between atoms.

V. CONCLUSION

In summary, we investigate the performance of “+ U ” correction in high pressure based on the widely-used augmented methods (PAW and LAPW) systematically. Our work exhibits two previously unnoticed but vital phenomena in the high-pressure simulation of DFT+ U , and highlights the necessity of checking the applicability for DFT+ U simulation based on PAW for high-pressure conditions.

On the one hand, we found that the force can be seriously underestimated in high-pressure (over 100 GPa) with DFT+ U in VASP based on the PAW method. The underestimation can be even up to 50% comparing with the pressure calculated from DFT+ U in WIEN2k based on LAPW and HSE06 based on PAW. Through delicate analysis, we point out that the larger range of projection operator usually used in PAW of VASP than that in LAPW of WIEN2k should be the main cause of the different behavior of “+ U ” correction in these two methods. The large augmented range in PAW makes the overlap of local orbitals. And the overlap leads to an occupation

more than 1.0 in the high-pressure condition. From our investigation, it is caused by the normalization problem of local orbital in small volume, which implies the over occupation is unphysical. The over occupation makes the $4f$ -local orbitals of PAW in VASP lose the radial feature of $4f$, and weakens the reliability of the DFT+ U method in high-pressure conditions. Thus, we propose that the “+ U ” correction should be carefully checked before applying to the simulation of high-pressure condition.

On the other hand, an unusual behavior of the pressure simulation between DFT and correlation correction methods (DFT+ U and HSE06) is observed at high pressure. The pressure predicted from correlation correction methods is unexpectedly lower than that from DFT at the same volume for some heavy lanthanides (Tm, Yb and Lu). We explained the phenomenon from the aspect that the electron in interatomic region is stabilized in correction methods comparing with DFT. However, it is just a preliminary explanation, and more detailed investigations are required for a more clearly understanding. For further investigation, researchers should put efforts on the solvation of the unphysical behavior of PAW in high pressure and the profound understanding of the softening in correction methods. There are still some other factors not considered in our work, such as spin polarization, spin-orbit coupling, phase transition and so on. Their influence should be studied in the following researches.

VI. ACKNOWLEDGEMENT

We thank Yuan-Ji Xu, Hua-Jie Chen, Bo Sun, He-Guang Mao, Xing-Jie Han and Dan Jian for helpful discussions. The work was supported by the National Nature Science Foundation of China (No.U1930401, NO.12004048 and No.11971066), the Science Challenge Project (Grant No.TZ2018002), the National Key R&D Program of China 2021YFB3501503 and the Foundation of LCP. We thank the Tianhe platforms at the National Supercomputer Center in Tianjin.

VII. APPENDIX

A. Projection operator in LAPW

In the frame of LAPW, the projection operator acts on the single electron orbital $\psi_i(\mathbf{r})$ to obtain local density matrix, which has the formation like,

$$n_{mm'} = \sum_{i \in occ.} \int d\mathbf{r} d\mathbf{r}' \psi_i^*(\mathbf{r}) \hat{P}_{mm'}(\mathbf{r}, \mathbf{r}') \psi_i(\mathbf{r}') \quad (17)$$

$n_{mm'}$ is the element of matrix with quantum number m and m' . The summation over all electron orbitals i , which are occupied. In LAPW methods, the radial part of the projection operator is determined by the radial

part of the augmented wave function and is truncated by the radius of augmented range. Thus $\hat{P}_{mm'}(\mathbf{r}, \mathbf{r}')$ only extract the information of subspace by the angular part. The $\hat{P}_{mm'}(\mathbf{r}, \mathbf{r}')$ can be written as,

$$\hat{P}_{mm'}(\mathbf{r}, \mathbf{r}') = \frac{1}{r^2} \theta_\alpha(r) \delta(r - r') Y_{lm'}^*(\hat{\mathbf{r}}') Y_{lm}(\hat{\mathbf{r}}) \quad (18)$$

$\theta_\alpha(r)$ is a step function which is 1 within the augmented range α , and is 0 outside. $\delta(r - r')$ is a delta function. $Y_{lm}(\hat{\mathbf{r}})$ is the spherical harmonic with angular momentum l, m . Since $\hat{P}_{mm'}(\mathbf{r}, \mathbf{r}')$ do not specify the feature of the radial part of local orbital, it is important to show the form of radial wave function if LAPW orbitals. Here shows a basis with reciprocal coordinate $\mathbf{k} + \mathbf{G}$

$$\begin{aligned} \phi_{\mathbf{k}+\mathbf{G}}(\mathbf{r}) &= \theta_I(\mathbf{r}) \Omega^{-\frac{1}{2}} \exp(i(\mathbf{k} + \mathbf{G}) \cdot \mathbf{r}) \\ &+ \sum_{\alpha lm} \theta_\alpha(\mathbf{r}) [A_{\alpha lm}^{\mathbf{k}+\mathbf{G}} u_{\alpha l}(r_\alpha) + B_{\alpha lm}^{\mathbf{k}+\mathbf{G}} \dot{u}_{\alpha l}(r_\alpha)] Y_{lm}(\hat{\mathbf{r}}_\alpha) \end{aligned} \quad (19)$$

α and I stand for the augmented and interval ranges respectively. $\theta_I(\mathbf{r})$ and $\theta_\alpha(\mathbf{r})$ are the step function, which makes corresponding restricted in the certain range. In the interval range, the plane wave is used. In augmented spherical range an atom-like wave function is used. $u_{\alpha l}(r_\alpha)$ and $\dot{u}_{\alpha l}(r_\alpha)$ are the solution of radial Schrodinger function at certain energy with spherical averaged KS potential and its derivative function to energy respectively. The KS single electron orbital can be described by a set of these basis.

$$\psi_i(\mathbf{r}) = \sum_{\mathbf{G}} C_{\mathbf{G}}^i \phi_{i, \mathbf{G}}(\mathbf{r}) \quad (20)$$

The summation is over reciprocal lattice \mathbf{G} . i stands for the order of KS orbital. Thus, in the augmented range, the KS orbital is

$$\psi_i(\mathbf{r}) = \sum_{lm} [\mathcal{A}_{\alpha lm}^i u_{\alpha l}(r) + \mathcal{B}_{\alpha lm}^i \dot{u}_{\alpha l}(r)] Y_{lm}(\hat{\mathbf{r}}) \quad (21)$$

with $\mathcal{A}_{\alpha lm}^i = \sum_{\mathbf{G}} C_{\mathbf{G}}^i A_{\alpha lm}^{i, \mathbf{G}}$ and $\mathcal{B}_{\alpha lm}^i = \sum_{\mathbf{G}} C_{\mathbf{G}}^i B_{\alpha lm}^{i, \mathbf{G}}$. Since $\langle u_i | u_i \rangle = 1$ and $\langle u_i | \dot{u}_i \rangle = 0$ in LAPW method,

the element of local density matrix is

$$n_{mm'} = \sum_{i \in occ.} \mathcal{A}_{\alpha lm}^i [\mathcal{A}_{\alpha lm'}^i]^* + \mathcal{B}_{\alpha lm}^i [\mathcal{B}_{\alpha lm'}^i]^* \langle \dot{u}_l | \dot{u}_l \rangle \quad (22)$$

B. Projection operator in PAW

PAW is another important augmented method. The formation of the local density matrix and projection operator is the same as the ones in LAPW methods. The difference of the element in the local density matrix between PAW and LAPW comes from the different radial orbital of these two methods. In PAW, the KS orbital has the form,

$$|\psi_i\rangle = |\tilde{\psi}_i\rangle + \sum_s (|\phi_s\rangle - |\tilde{\phi}_s\rangle) \langle \tilde{p}_s | \tilde{\psi}_i \rangle \quad (23)$$

$|\phi_s\rangle$ and $|\tilde{\phi}_s\rangle$ are also atom-like orbitals with the form,

$$|\phi_s\rangle = R_s(r) Y_s(\hat{\mathbf{r}}) \quad (24)$$

$$|\tilde{\phi}_s\rangle = \tilde{R}_s(r) Y_s(\hat{\mathbf{r}}) \quad (25)$$

Subscript s is a collection of angular momentum lm , atom site α and the order of radial function t . With the definition, the element of local density matrix in PAW is

$$\begin{aligned} n_{mm'} &= \sum_{i \in occ.} \langle \psi_i | \hat{P}_{mm'} | \psi_i \rangle \\ &= \sum_{i \in occ.} \sum_{t_1 t_2} \langle \tilde{\psi}_i | \tilde{p}_{m t_1} \rangle \langle \phi_{m t_1} | \mathbf{P}_{mm'} | \phi_{m' t_2} \rangle \langle \tilde{p}_{m' t_2} | \tilde{\psi}_i \rangle \\ &= \sum_{t_1 t_2} \rho_{mm'}^{t_1 t_2} \langle R_{t_1} | R_{t_2} \rangle \end{aligned} \quad (26)$$

and

$$\rho_{mm'}^{t_1 t_2} = \sum_{i \in occ.} \langle \tilde{\psi}_i | \tilde{p}_{m t_1} \rangle \langle \tilde{p}_{m' t_2} | \tilde{\psi}_i \rangle \quad (27)$$

* Electronic address: liu_yu@iapcm.ac.cn

† Electronic address: song_haifeng@iapcm.ac.cn

¹ A. V. Bushman. Intense Dynamic Loading of Condensed Matter (CRC Press, 1992).

² R. P. Feynman, N. Metropolis, and E. Teller. Equations of State of Elements Based on the Generalized Fermi-Thomas Theory. *Phys. Rev.*, 75, 1561, 1949.

³ S. L. McCarthy. The Kirzhnits Corrections to the Thomas-Fermi Equation of State, 1965.

⁴ D. A. Kirzhnits, Y. E. Lozovik, and G. V. Shpatakovskaya. Statistical Model of Matter. *Sov. Phys. Uspekhi* 18, 649, 1975.

⁵ H. Liu, H. Song, Q. Zhang, G. Zhang, and Y. Zhao. Val-

idation for Equation of State in Wide Regime: Copper as Prototype, *Matter Radiat. Extrem.* 1, 123, 2016.

⁶ D. A. Young, H. Cynn, P. Söderlind, and A. Landa. Zero-Kelvin Compression Isotherms of the Elements $1 \leq Z \leq 92$ to 100 GPa. *J. Phys. Chem. Ref. Data* 45, 043101, 2016.

⁷ H.-F. Song, H.-F. Liu, G.-C. Zhang, Y.-H. Zhao. Numerical Simulation of Wave Propagation and Phase Transition of Tin under Shock-Wave Loading. *Chin. Phys. Lett.* 26, 066401, 2009.

⁸ H.-F. Song, H.-F. Liu. Theoretical Study of Thermodynamic Properties of Metal Be. *Acta Phys. Sin.* 5, 2007.

⁹ V. B. Grasso. Rare Earth Elements in National Defense: Background, Oversight Issues, and Options for Congress,

- in (Library Of Congress Washington DC Congressional Research Service, 2013).
- ¹⁰ G. K. Samudrala and Y. K. Vohra. Structural Properties of Lanthanides at Ultra High Pressure, in Handbook on the Physics and Chemistry of Rare Earths, Vol. 43 (Elsevier, 2013), pp. 275–319.
 - ¹¹ S. E. Finnegan, C. V. Storm, E. J. Pace, M. I. McMahon, S. G. MacLeod, E. Plekhanov, N. Bonini, and C. Weber. High-Pressure Structural Systematics in Neodymium up to 302 GPa. *Phys. Rev. B* 103, 134117, 2021.
 - ¹² C. S. Perreault and Y. K. Vohra. Static Compression of Rare Earth Metal Holmium to 282 GPa. *High Press. Res.* 40, 392, 2020.
 - ¹³ H. Sun, D. Kang, J. Dai, W. Ma, L. Zhou, and J. Zeng. First-Principles Study on Equation of States and Electronic Structures of Shock Compressed Ar up to Warm Dense Regime. *J. Chem. Phys.* 144, 124503, 2016.
 - ¹⁴ T. Tsuchiya. First-Principles Prediction of the P-V-T Equation of State of Gold and the 660-Km Discontinuity in Earth’s Mantle: First-Principles Prediction of Equation of State of Gold. *J. Geophys. Res. Solid Earth.* 108, 2003.
 - ¹⁵ S. Zhang, K. P. Driver, F. Soubiran, and B. Militzer. Equation of State and Shock Compression of Warm Dense Sodium—A First-Principles Study. *J. Chem. Phys.* 146, 074505, 2017.
 - ¹⁶ R. M. Martin. Electronic Structure: Basic Theory and Practical Methods (Cambridge University Press, Cambridge, UK; New York, 2004).
 - ¹⁷ A. Jain, Y. Shin, and K. A. Persson. Computational Predictions of Energy Materials Using Density Functional Theory. *Nat. Rev. Mater.* 1, 15004, 2016.
 - ¹⁸ P. Söderlind and D. Young. Assessing Density-Functional Theory for Equation-Of-State. *Computation* 6, 13, 2018.
 - ¹⁹ T. Zhang, Y. Wang, J. Xian, S. Wang, J. Fang, S. Duan, X. Gao, H. Song, and H. Liu. Effect of the Projector Augmented Wave Potentials on the Simulation of Thermodynamic Properties of Vanadium. *Matter Radiat. Extrem.* 6, 068401, 2021.
 - ²⁰ M. Weinert. Solution of Poisson’s Equation: Beyond Ewald-type Methods. *J. Math. Phys.* 22, 2433, 1981.
 - ²¹ E. Wimmer, H. Krakauer, M. Weinert, and A. J. Freeman. Full-Potential Self-Consistent Linearized-Augmented-Plane-Wave Method for Calculating the Electronic Structure of Molecules and Surfaces: O₂ Molecule, *Phys. Rev. B* 24, 864, 1981.
 - ²² D. Vanderbilt. Soft Self-Consistent Pseudopotentials in a Generalized Eigenvalue Formalism. *Phys. Rev. B* 41, 7892, 1990.
 - ²³ P. E. Blöchl. Projector Augmented-Wave Method. *Phys. Rev. B* 50, 17953, 1994.
 - ²⁴ P. Blaha, K. Schwarz, F. Tran, R. Laskowski, G. K. H. Madsen, and L. D. Marks. WIEN2k: An APW+lo Program for Calculating the Properties of Solids. *J. Chem. Phys.* 152, 074101, 2020.
 - ²⁵ J. K. Dewhurst et al. The Elk Code, elk.sourceforge.net.
 - ²⁶ G. Kresse and D. Joubert. From Ultrasoft Pseudopotentials to the Projector Augmented-Wave Method. *Phys. Rev. B* 59, 1758, 1999.
 - ²⁷ P. Giannozzi, O. Barone, P. Bonfà, D. Brunato, R. Car, I. Carnimeo, C. Cavazzoni, S. de Gironcoli, P. Delugas, F. Ferrari Ruffino, A. Ferretti, N. Marzari, I. Timrov, A. Urru, and S. Baroni. QUANTUM ESPRESSO toward the Exascale. *J. Chem. Phys.* 152, 154105, 2020.
 - ²⁸ J. Enkovaara, C. Rostgaard, J. J. Mortensen, J. Chen, M. Dulak, L. Ferrighi, J. Gavnholt, C. Glinsvad, V. Haikola, H. A. Hansen, H. H. Kristoffersen, M. Kuisma, A. H. Larsen, L. Lehtovaara, M. Ljungberg, O. Lopez-Acevedo, P. G. Moses, J. Ojanen, T. Olsen, V. Petzold, N. A. Romero, J. Stausholm-Møller, M. Strange, G. A. Tritsarlis, M. Vanin, M. Walter, B. Hammer, H. Häkkinen, G. K. H. Madsen, R. M. Nieminen, J. K. Nørskov, M. Puska, T. T. Rantala, J. Schiøtz, K. S. Thygesen, and K. W. Jacobsen. Electronic Structure Calculations with GPAW: A Real-Space Implementation of the Projector Augmented-Wave Method. *J. Phys. Condens. Matter* 22, 253202, 2010.
 - ²⁹ X. Gonze, B. Amadon, G. Antonius, F. Arnardi, L. Baguet, J.-M. Beuken, J. Bieder, F. Bottin, J. Bouchet, E. Bousquet, N. Brouwer, F. Bruneval, G. Brunin, T. Cavignac, J.-B. Charraud, W. Chen, M. Côté, S. Cottenier, J. Denier, G. Geneste, P. Ghosez, M. Giantomassi, Y. Gillet, O. Gingras, D. R. Hamann, G. Hautier, X. He, N. Helbig, N. Holzwarth, Y. Jia, F. Jollet, W. Lafargue-Dit-Hauret, K. Lejaeghere, M. A. L. Marques, A. Martin, C. Martins, H. P. C. Miranda, F. Naccarato, K. Persson, G. Petretto, V. Planes, Y. Pouillon, S. Prokhorenko, F. Ricci, G.-M. Rignanese, A. H. Romero, M. M. Schmitt, M. Torrent, M. J. van Setten, B. Van Troeye, M. J. Verstraete, G. Zerah, and J. W. Zwanziger. The Abinitproject: Impact, Environment and Recent Developments. *Comput. Phys. Commun.* 248, 107042, 2020.
 - ³⁰ N. A. W. Holzwarth, G. E. Matthews, R. B. Dunning, A. R. Tackett, and Y. Zeng. Comparison of the Projector Augmented-Wave, Pseudopotential, and Linearized Augmented-Plane-Wave Formalisms for Density-Functional Calculations of Solids. *Phys. Rev. B* 55, 2005, 1997.
 - ³¹ A. B. Shick, A. I. Liechtenstein, and W. E. Pickett. Implementation of the LDA+U Method Using the Full-Potential Linearized Augmented Plane-Wave Basis. *Phys. Rev. B* 60, 10763, 1999.
 - ³² V. I. Anisimov, F. Aryasetiawan, and A. I. Liechtenstein. First-Principles Calculations of the Electronic Structure and Spectra of Strongly Correlated Systems: The LDA + U Method. *J. Phys. Condens. Matter* 9, 767, 1997.
 - ³³ A. I. Liechtenstein, V. I. Anisimov, and J. Zaanen. Density-Functional Theory and Strong Interactions: Orbital Ordering in Mott-Hubbard Insulators. *Phys. Rev. B* 52, R5467, 1995.
 - ³⁴ M. E. Arroyo-de Dompablo, A. Morales-García, and M. Taravillo. DFT+ U Calculations of Crystal Lattice, Electronic Structure, and Phase Stability under Pressure of TiO₂ Polymorphs. *J. Chem. Phys.* 135, 054503, 2011.
 - ³⁵ B. Himmetoglu, A. Floris, S. de Gironcoli, and M. Cococcioni. Hubbard-Corrected DFT Energy Functionals: The LDA+U Description of Correlated Systems. *Int. J. Quantum Chem.* 114, 14, 2014.
 - ³⁶ X. Deng, X. Dai, and Z. Fang. LDA + Gutzwiller Method for Correlated Electron Systems. *EPL Europhys. Lett.* 83, 37008, 2008.
 - ³⁷ V. Anisimov and Y. Izyumov. Electronic Structure of Strongly Correlated Materials (Springer-Verlag, Berlin Heidelberg, 2010).
 - ³⁸ A. Avella and F. Mancini. Strongly Correlated Systems. Theoretical Methods (Springer, Heidelberg; New York, 2012).
 - ³⁹ M. Casadei, X. Ren, P. Rinke, A. Rubio, and M. Scheffler. Density Functional Theory Study of the $\alpha - \gamma$ Phase Transition in Cerium: Role of Electron Correlation and

- f*-Orbital Localization. *Phys. Rev. B* 93, 075153, 2016.
- ⁴⁰ J. P. Perdew, M. Ernzerhof, and K. Burke. Rationale for Mixing Exact Exchange with Density Functional Approximations. *J. Chem. Phys.* 105, 9982, 1996.
- ⁴¹ H. Jiang. First-Principles Approaches for Strongly Correlated Materials: A Theoretical Chemistry Perspective. *Int. J. Quantum Chem.* 115, 722, 2015.
- ⁴² M. Rahm and N. V. Skorodumova. Phase Stability of the Rare-Earth Sesquioxides under Pressure. *Phys. Rev. B* 80, 104105, 2009.
- ⁴³ P. Modak and A. K. Verma. First-Principles Investigations of Equation of States and Phase Transitions in PaN under Pressure. in (Indian Institute of Technology, Bombay, Mumbai, India, 2013), pp. 80–81.
- ⁴⁴ P. Steneteg, B. Alling, and I. A. Abrikosov. Equation of State of Paramagnetic CrN from Ab Initio Molecular Dynamics. *Phys. Rev. B* 85, 144404, 2012.
- ⁴⁵ H. Hsu, K. Umemoto, M. Cococcioni, and R. M. Wentzcovitch. The Hubbard U Correction for Iron-Bearing Minerals: A Discussion Based on (Mg,Fe)SiO₃ Perovskite. *Phys. Earth Planet. Inter.* 185, 13, 2011.
- ⁴⁶ G. Rollmann, P. Entel, A. Rohrbach, and J. Hafner. High-Pressure Characteristics of α -Fe₂O₃ Using DFT+U. *Phase Transit.* 78, 251, 2005.
- ⁴⁷ H. Y. Geng, Y. Chen, Y. Kaneta, and M. Kinoshita. Structural Behavior of Uranium Dioxide under Pressure by LSDA + U Calculations. *Phys. Rev. B* 75, 054111, 2007.
- ⁴⁸ Z. Song, J. J. Yang, and J. S. Tse. A Comparative Study on the LDA + U and Hybrid Functional Methods on the Description of the Electronic Structure of YTiO₃ under High Pressure. *Can. J. Chem.* 87, 1374, 2009.
- ⁴⁹ P. Zhang, B.-T. Wang, and X.-G. Zhao. Ground-State Properties and High-Pressure Behavior of Plutonium Dioxide: Density Functional Theory Calculations. *Phys. Rev. B* 82, 144110, 2010.
- ⁵⁰ X.-D. Wen, R. L. Martin, G. E. Scuseria, S. P. Rudin, E. R. Batista, and A. K. Burrell. Screened Hybrid and DFT + U Studies of the Structural, Electronic, and Optical Properties of U₃O₈. *J. Phys. Condens. Matter* 25, 025501, 2013.
- ⁵¹ L. Zhou, F. Körmann, D. Holec, M. Bartosik, B. Grabowski, J. Neugebauer, and P. H. Mayrhofer. Structural Stability and Thermodynamics of CrN Magnetic Phases from Ab Initio Calculations and Experiment *Phys. Rev. B* 90, 184102, 2014.
- ⁵² Y.-C. Wang, Z.-H. Chen, and H. Jiang. The Local Projection in the Density Functional Theory plus U Approach: A Critical Assessment. *J. Chem. Phys.* 144, 144106, 2016.
- ⁵³ J. P. Perdew, K. Burke, and M. Ernzerhof. Generalized Gradient Approximation Made Simple. *Phys. Rev. Lett.* 77, 3865, 1996.
- ⁵⁴ H. Jiang, R. I. Gomez-Abal, P. Rinke, and M. Scheffler. Localized and Itinerant States in Lanthanide Oxides United by GW @ LDA + U. *Phys. Rev. Lett.* 102, 2009.
- ⁵⁵ J. B. Morée and B. Amadon. First-Principles Calculation of Coulomb Interaction Parameters for Lanthanides: Role of Self-Consistency and Screening Processes. *Phys. Rev. B* 98, 205101, 2018.
- ⁵⁶ J. Heyd, G. E. Scuseria, and M. Ernzerhof. Hybrid Functionals Based on a Screened Coulomb Potential. *J. Chem. Phys.* 118, 8207, 2003.
- ⁵⁷ S. Ryee and M. J. Han. The Effect of Double Counting, Spin Density, and Hund Interaction in the Different DFT+U Functionals. *Sci. Rep.* 8, 9559, 2018.
- ⁵⁸ D. D. O'Regan, N. D. M. Hine, M. C. Payne, and A. A. Mostofi. Linear-scaling DFT + U with full local orbital optimization. *Phys. Rev. B* 85, 085107, 2012.
- ⁵⁹ O. Bengone, M. Alouani, P. Blöchl, and J. Hugel. Implementation of the Projector Augmented-Wave LDA+U Method: Application to the Electronic Structure of NiO. *Phys. Rev. B* 62, 16392, 2000.
- ⁶⁰ M. Cococcioni and S. de Gironcoli. Linear Response Approach to the Calculation of the Effective Interaction Parameters in the LDA + U Method. *Phys. Rev. B* 71, 2005.
- ⁶¹ E. R. Ylvisaker, DFT and DMFT: Implementations and Applications to the Study of Correlated Materials, 178 (n.d.).
- ⁶² J. Yu, M. Zhang, Z. Zhang, S. Wang and Y. Wu, Hybrid-functional calculations of electronic structure and phase stability of MO (M = Zn, Cd, Be, Mg, Ca, Sr, Ba) and related ternary alloy M_xZn_{1-x}O *RSC Adv.* 9, 2019.
- ⁶³ C. Loschen, J. Carrasco, K. M. Neyman and F. Illas, First-principles LDA + U and GGA + U study of cerium oxides: Dependence on the effective U parameter *Phys. Rev. B* 75, 2007.